LAWRENCE
LIVERMORE
NATIONAL
LABORATORY

LLNL-JRNL-501357

Modeling Noble Gas Transport and Detection for The Comprehensive Nuclear-Test-Ban Treaty

Y. Sun, C. R. Carrigan

September 27, 2011

Modeling Noble Gas Transport and Detection for The Comprehensive Nuclear-Test-Ban Treaty

Disclaimer

Modeling Noble Gas Transport and Detection for The Comprehensive Nuclear-Test-Ban Treaty

YUNWEI SUN[1] and CHARLES R. CARRIGAN[1]

Abstract – Detonation gases released by an underground nuclear test include trace amounts of ^{133}Xe and ^{37}Ar. In the context of the Comprehensive Nuclear Test Ban Treaty (CTBT) On Site Inspection protocol, such gases released from or sampled at the soil surface could be used to indicate the occurrence of an explosion in violation of the Treaty. To better estimate the levels of detectability from an underground nuclear test(UNE), we developed mathematical models to evaluate the processes of ^{133}Xe and ^{37}Ar transport in fractured rock. Two models are developed respectively for above-boiling and below-boiling tests. When the temperature is below the boiling point and the subsurface system is sufficiently dry, the system is described using a single-gas-phase transport model and the barometric pumping becomes the major driving force to deliver ^{133}Xe and ^{37}Ar to ground surface. A above-boiling test is simulated using a two-phase and multi-component transport model. In the model, steam production and bubble expansion are the major processes driving noble gas components to ground surface. After the temperature in the chimney drops below boiling, barometric pumping takes over the role as the major transport process.

Keywords: Noble gas, transport, CTBT, detection, modeling

1. Introduction

Noble gas isotopes, such as ^{133}Xe and ^{37}Ar, have been studied for detection of nuclear explosions for the Comprehensive nuclear-Test-Ban Treaty (CTBT, Bowyer et al., 2002). Because of their short half-lives, the ambient background concentrations for those gas components are extremely low (Dresel and Waichler, 2004). The International Monitoring System (IMS) has developed the measurement sensitivity for ^{133}Xe better than 1 mBq m^{-3}. However, in addition to nuclear explosions, radioxenon isotopes may be produced and released from civil events. To better understand under what geohydrologic conditions the Xe and Ar signals will reach the surface in detectable amounts and to better estimate the value of subsurface noble gas sampling during an On Site Inspection, the transport mechanisms from a underground nuclear test to ground surface have to be studied.

Gas-phase transport has been studied for various purposes (Webb, 1996; Wu et al., 1998; Tidwell 2006; Pruess 2006). The barometric-pumping phenomenon has been identified as a driving force for gas-phase transport in the subsurface system (Nilson et al., 1991; Lindstrom et al., 1994; Wyatt et al., 1995; Carrigan et al., 1996; Auer et al., 1996; Martinez and Nilson 1999; Neeper 2001; 2002; Rossabi, 2006). The gas-phase advection in response to the pressure oscillation at ground surface behaves as cyclical "breathing" or push-pull gas flow through the permeable alluvia or fractures. Diffusive exchange between fractures and rock matrix dampens and delays the signature of gas concentrations at ground surface (Carrigan et al., 1996).

In addition to these breathing processes that have been studied, we developed a single-gas transport model and two-phase multi-component transport model to study a below-boiling test and a above-boiling test, respectively. In the single-gas model, we quantitatively studied the detectability and how the overburden alluvia affect the concentration signal at ground

[1]Lawrence Livermore National Laboratory, Livermore, CA 94550, USA. E-mail: sun4@llnl.gov

surface. In the above-boiling model, we demonstrated how the phase change and heat-pipe phenomena affect the gas-phase transport and how to capture the concentration signal at or near ground surface.

2. Physical Systems

The physical processes that control noble gas migration from the working point of a nuclear detonation to ground surface are complex and interdependent. In an underground nuclear explosion, vaporization and compression of geologic media will create and expand an open, approximately spherical cavity surrounding the working point. The cavity reaches its full size within a fraction of a second after detonation. The cavity radius is a function of the energy of the detonation, its depth of burial, and the strength of overlying geologic units (Carle et al., 2008). A steam bubble, together with radionuclides including noble gas isotopes, is formed and initially well contained within the cavity because of the highly compressed and impermeable cavity wall. Afterwards, steam-driven fractures (hydro-fractures) may be propagated from the cavity into the surrounding area and significantly reduce the cavity pressure. When the pressure within the cavity drops below the pressure resulting from the overburden rock, the cavity may collapse into the cavity creating a rubblized chimney, where radioactive gases are re-distributed over the void volume of the chimney. Under the conditions of thermally driven convection from the working point and barometric pressure oscillation at the ground surface, noble gas nuclides migrate upward toward the ground surface and make dectection possible.

2.1. Definition of Detectability

The success of noble gas detection from an underground nuclear test depends on the gas transport in the geological system. The geological structure, as well as many physical and chemical properties, controls the concentration profile of gas nuclides at and near ground surface. Taking the geological model of Carrigan et al. (1996) as an example, if the detection sensitivity (threshold) for xenon-133 is 1 mBq m^{-3} (Auer et al., 2004; 2010; Saey et al., 2009), as shown in Figure 1, the detectability can be characterized by (1) arrival time; (2) detection window width; and (3) detection window height (above the threshold). The arrival time, which is mainly determined by diffusivity of gas nuclides in the rock matrix and permeability in fractures, is defined as the time when the concentration of the noble gas component of the soil gas reaches its detection threshold. The detection window width is the time duration between the arrival time and the time when the concentration drops below the threshold. The window height is measured as the order of magnitude of the peak concentration exceeding the threshold. For a given radionuclide with a specfic half-life (e.g., 5.24 days of ^{133}Xe), monitoring is expected to be conducted within its detection window.

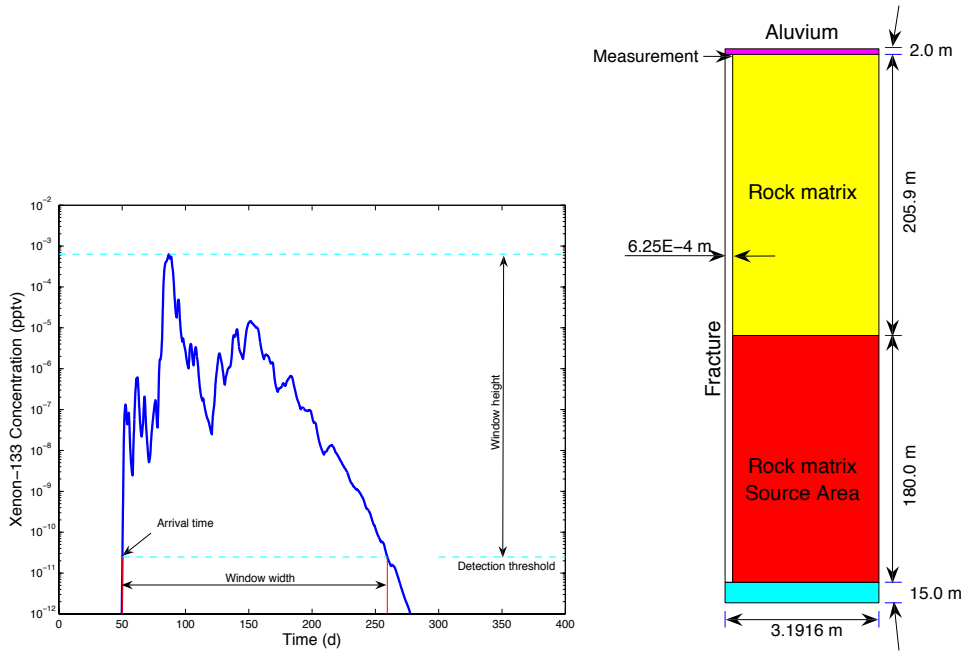

(a) (b)

Figure 1. Study domain of single-gas-phase transport for the Non-Proliferation Experiment. (a) An example of xenon-133 concentration history at the outlet of the fracture. (b) Geometry of study domain. Note that the horizontal dimension is exaggerated.

2.2. Non-Proliferation Experiment

The Non-Proliferation Experiment (NPE) detonated on September 22 in 1993, was a low-yield chemical explosion (Carrigan et al., 1996). The NPE was conducted the south-central N-Tunnel below the surface of Rainier Mesa. Gas components, ^{3}He and sulfur hexafluoride (SF_6) were released at the source (433.4 m depth) and monitored over approximately 500 days. The experimental data suggested that ^{133}Xe and ^{37}Ar would have been detectable after the detonation (Carrigan et al., 1996). A discrete fracture model was developed to describe the transport of ^{3}H and SF_6. In this study, we replace stable gas components, ^{3}H and SF_6 with decaying isotopes, ^{133}Xe and ^{37}Ar, in the numerical model and investigate the detectability.

2.3. Rainier Test

The Rainier test, which was conducted on September 19, 1957, is considered as the first fully contained underground test (Tompson et al., 2010). In the years following the test, extensive reentry mining and drilling operations were undertaken to characterize the cavity and altered environment.

The Non-Proliferation Experiment, which was detonated near the Rainier test, was conducted to study the transport of gas-phase components in the fractured rock. Although both the Rainier and the NPE tests were conducted in the same bedded tuff system, they are considered as above-boiling and below-boiling tests. In the above-boiling test the residual heat produced by a nuclear detonation alters the themohydrological condition, which in turn becomes the dominant driving force for gas-phase transport. Without considering the test-induced heat, the barometric pumping on the ground surface is the only driving force for the

NPE chemical test. A full-scale Rainier-test model is developed to understand (1) the physical processes that affect the gas-phase radionuclide redistribution under transient pressure and temperature conditions; (2) the effects of variably saturated conditions on gas-phase radionuclide transport under thermal conditions; (3) the role of fracture-matrix interactions and matrix diffusion; and (4) the role of barometric pumping on noble gas detection.

3. Conceptual Models

Two conceptual models are presented in this section. The Non-Proliferation Experiment for ^{133}Xe transport is described as an isothermal and single-gas-phase transport in rock matrix with a discrete fracture. The Rainier Test is described using a two-phase and four-component (water, air, ^{133}Xe, and ^{37}Ar) transport under thermal conditions in a dual-permeability domain.

3.1. Conceptual Model of NPE

As shown in Figure 1(b), a single vertical fracture penetrates the rock matrix. The fracture aperture size is based on the mean value of estimated aperture size and matrix block size ((i.e., distance between fractures)) is estimated using the fracture frequency. An alluvial layer of 2 m is over lain on the top of fractured rock. It is assumed that both heat and radionuclides are distributed over the rock-matrix source area and the thermal effect on gas-phase transport remains minimal. The liquid saturation is assumed to be constant between the working point and ground surface and does not affect gas-phase permeability. Therefore, the physical system is conceptualized as a single gas-phase transport under isothermal condition. Detailed description about rock properties, initial and boundary conditions, and model grids is referred to Carrigan et al. (1996). Three uncertain parameters, aperture size of fracture, permeability in alluvium, and gas diffusivity in rock matrix are considered to characterize the detectability indices, arrival time and detection window size.

3.2. Conceptual Model of Rainier Test

The Rainier-test is simulated using a sequence of separate yet continuous models that represent multiple-phase flow under thermal conditions in the fractured rock environment surrounding the test cavity and chimney. The models are developed in a two-dimensional, radial symmetric geometry and are based on a modeling domain extending from the ground surface to the water table and extending a significant distance away radially (1000 m) from the vertical axis passing through the working point. Then, the assumption of the ambient thermal abnd hydrologic condition is justified at the outer boundary.

The use of distinct model stages for the Rainier test allows important aspects of the thermohydrologic dynamics and evolution to be addressed over periods (1) before detonation, (2) after detonation and before chimney collapse, and (3) after chimney collapse. Transition between the stages involves the changing material domains and the mapping of initial conditions. The pre-test model is used to produce the ambient thermal and hydrologic conditions, under which internally consistent and steady-state saturation, pressure, and temperature conditions are simulated for one million years within an unaltered system before detonation to reach equilibrium. The pre-test model is considered as the conversion from a boundary-value problem to a steady-state condition. The test model is designed to present the processes after the detonation and before the chimney collapse. A spherical cavity, which holds explosively produced thermal energy, pressure, and radionuclides, is imbedded in the model grids. The post-collapse model is designed to examine the longer-term gas-phase transport. The collapse causes reassignment of rock materials in the chimney domain and physical property alteration in the surrounding zone.

Differently from the NPE model, all models of Rainier test are based upon a non-isothermal, two-phase flow formulation involving water and air as principal components, and specifically considering xenon-133 and argon-37 as minor components in determining their migration and redistribution for quantifying the detectability. The fractured rock system is conceptualized as a dual continuum medium (fracture and matrix, DKM, Ho, 1997; Sun et al., 2010) and simulations were conducted using the NUFT code (Nitao, 1998).

3.3. Study Domain and Grids of Rainier Test Model

The study domain is composed of 17 geologic units, covers the entire unsaturated zone from ground surface to the water table, and includes the detailed geometry of the cavity, chimney, and altered zone, which were produced by the Rainier detonation. Grid-block sizes range from a few tens of centimeters around the chimney to tens of meters in the far field. As shown in Figure 2, the physical system is discretized in a radially-symmetric (cylindrical) coordinate system. The conceptual model is based on a dual-permeability presentation of overlapping fracture and matrix continua (Sun et al., 2010).

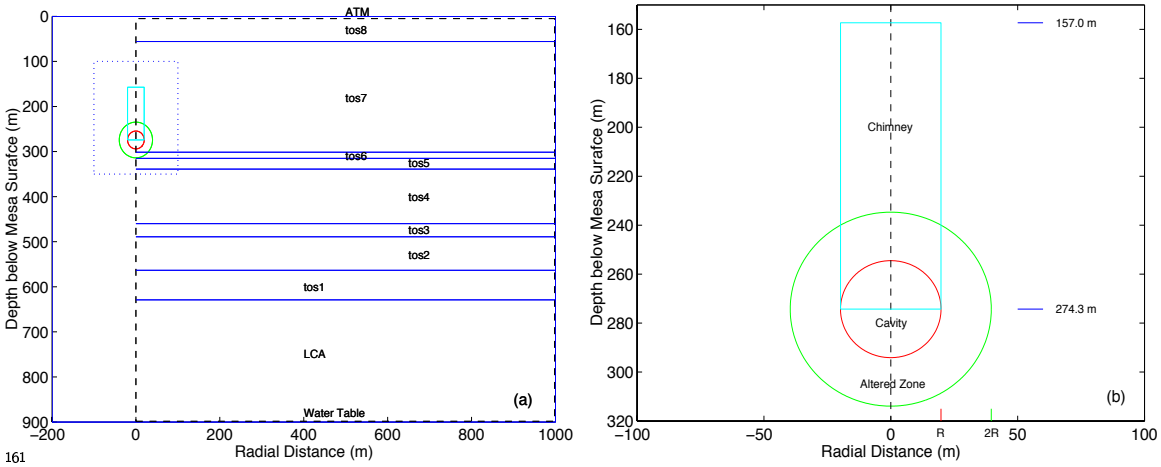

Figure 2. Study domain of the Rainier test model. (a) Vertical cross-section of the Rainier test model. "tos1", "tos2", ⋯, and "LCA" are geologic units where tos7 is subdivided into 9 subunits. The dashed line defines the study domain. (b) Local geometry of the cavity, chimney, and altered zone. The detonation location is at (0, 274.3), the cavity radius is 19.81 m, and the chimney height is 117.3 m between the depth of 157.0 m and the working point.

3.4. Physical Properties

Physical properties include component, phase, and rock properties. Rock properties include permeability, porosity, thermal conductivity, specific heat, and the van Genuchten parameters α, m, and residual saturation, to specify saturation-dependent gas and liquid permeability and capillary pressure (Sun et al., 2010).

3.4.1. Phase and Component Properties. The phase-equilibrium partitioning coefficient, K_{eq}, for a dissolved component in adjoining gas and liquid phases is defined as the ratio of its mole fractions in the gas phase, y, to its mole fraction in the liquid phase, x. A Clever gas solubility model (Clever, 1979; 1980) is applied to the gas phase-equilibrium relations for xenon-133 and argon-37 such that

$$K_{eq} = \frac{y}{x} = \frac{p_g^r}{S\, p_g} \tag{1}$$

where S is the mole fraction (solubility) of component xenon-133 or argon-37 dissolved in the liquid phase measured at the reference gas pressure, p_g^r, and p_g is the gas-phase pressure. The solubility is determined using experimental data as a function of temperature (Ekwurzel, 2004)

$$\ln S = A + \frac{B}{T_n} + C \ln T_n + F T_n \tag{2}$$

where A, B, C, and F are model parameters specific to xenon and argon, and T_n is the temperature in Kelvin divided by 100. The dependence of K_{eq} on temperature for xenon and argon is shown in Figure 3.

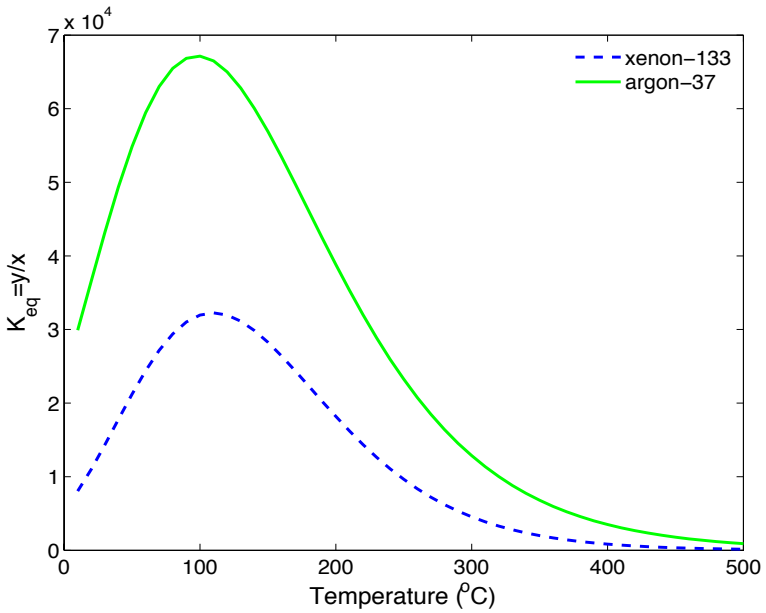

Figure 3. Phase-equilibrium coefficient of xenon-133 and argon-37 as a function temperature.

The free molecular diffusion coefficients in gas and liquid phases, D_g and D_l, can be modeled as a function of temperature, T_k (degrees Kelvin), and gas-phase pressure, p_g (Pa)

$$D_g = D_g^0 \frac{p_g^r}{p_g} \left(\frac{T_k}{273.15} \right)^{n_g}, \quad D_l = D_l^0 \left(\frac{T_k}{273.15} \right)^{n_l}. \tag{3}$$

The diffusion model parameters, D_g^0, D_l^0, n_g, and n_l should be fitted to experimental data. Because of the lack of experimental data for xenon and argon diffusion in gas phase, we estimate the D_g^0 accordingly to molecular mass of gas-phase components and assume n_g to be zero. This assumption may result in an underestimation of the gas-phase transport in the high temperature zone. The diffusivity model in liquid phase was fitted using the experimental data of Holocher et al. (2002). Equilibrium partitioning and free molecular diffusivity model parameters for noble gases are given in Table 2.

Table 1. Equilibrium partitioning and free molecular diffusivity model parameters for xenon and argon.

Component	A	B	C	F	D_g^0 $(10^{-5}\mathrm{m^2s^{-1}})$	n_g	D_l^0 $(10^{-9}\mathrm{m^2s^{-1}})$	n_l
Ar	-57.67	74.76	20.14	0.0	2.00	0.0	1.44	7.22
Xe	-74.74	105.21	27.47	0.0	1.24	0.0	0.66	9.25

3.4.2. Rock Properties. DKM rock properties are further categorized as medium-dependent hydrologic and thermal properties and partitioned physical properties (Buscheck et al., 2002). The hydrologic properties include relative permeability, porosity, van Genuchten α and m, residual saturation, and transition saturation (Sun et al., 2010). The maximum saturation of all materials is assumed to be 1.0. For the fracture medium, three additional parameters, fracture connectivity, fracture frequency, and specific interaction area between fracture and matrix media, are included. Single-continuum materials, such as alluvium, use the same properties in fracture and matrix.

Appropriate values for the tortousity factor are selected for the matrix and fracture continuum on the basis of the parameter range given by de Marsily (1986), which ranges from a value of 0.1 for clays to 0.7 for sands. A value of 0.2 is estimated for the matrix continuum because the pore sizes for the matrix are closer to that of clays than to that of sands. A value of 0.7 is assumed for the fracture continuum because the effective pore sizes for fractures are similar to those of sands. Tortousity factors are also estimated with a Millington model using residual saturation from the van Genuchten parameters (Nitao, 1998). The effective diffusion coefficient for gas-phase components is a linear function of the tortousity factor,

$$D_e = \tau\phi(1 - S_l)D_g \tag{4}$$

where τ is the tortousity factor, ϕ is the porosity, S_l is the liquid saturation, and D_g is the diffusion coefficient defined in (3).

3.4.3. Boundary/Initial Conditions. The ground surface and water table are considered to be the upper and lower boundaries of the Rainier Test models. At the ground surface boundary, gas-phase conditions are specified by the air composition and the liquid-phase saturation is fixed to be zero. At the water table boundary, liquid-phase conditions are specified based on ground water compositions with a full liquid saturation. Initial conditions between ground surface and water table are obtained by running the pre-test model using the specified boundary conditions, physical properties, and stratigraphy. Figure 4 shows a time series of the measured pressure and temperature at Rainier Mesa over 9,130-day period between January 1, 1983 and December 31, 2007. The data show the diurnal, annual, and daily variations. Pre-calibration exercise indicates that the variation of temperature does not significantly affect gas-phase flow while the daily variation of surface pressure significantly drives the push-pull processes between fractures and rock matrix. Therefore, the mean value of temperature over the NPE monitoring period (517 days), 9.98 °C is assumed as a constant temperature boundary at the surface.

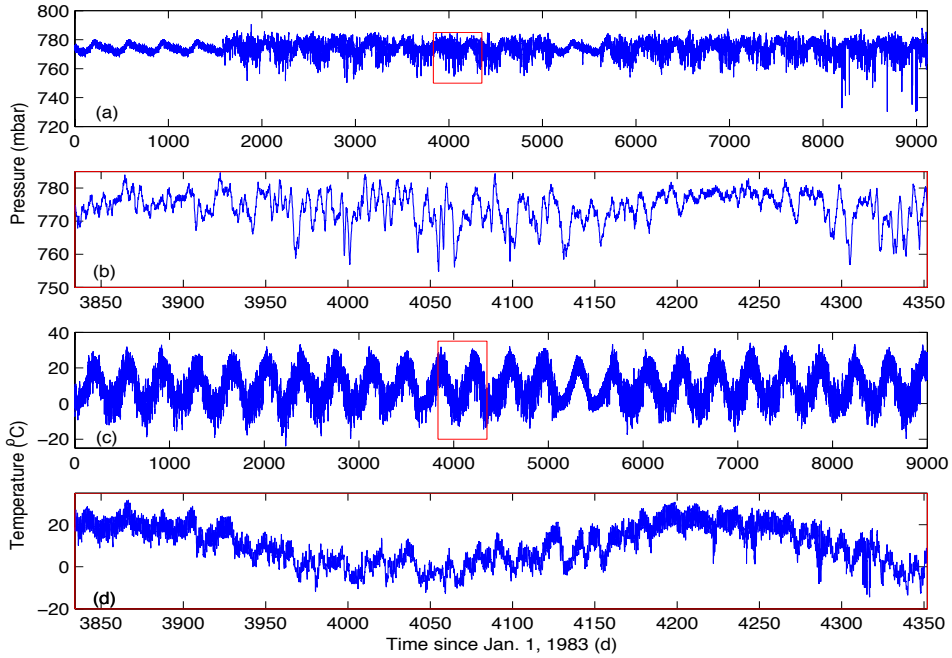

Figure 4. Barometric and temperature boundary conditions at ground surface. (a) Hourly pressure data from January 1, 1983 to December 31, 2007 (Tompson et al., 2010). (b) Hourly pressure data used in the NPE experiment (Carrigan et al., 1996). (c) Hourly temperature data from January 1, 1983 to December 31, 2007 (Tompson et al., 2010). (d) Hourly temperature data during the NPE experiment.

Two sets of temperature data are available for estimating thermal conductivities of 17 stratigraphic layers at the locations underneath Rainier Mesa. At shallow depth, temperature was measured from ground surface to the working point (274.3 m depth) in well UCRL-3 before the detonation (Warner and Violet, 1959). A more current measurement of 29.86 °C was obtained at the water table in nearby well ER-12-3 (Tompson et al., 2010). Taking 9.98 °C and 29.86 °C as boundary temperatures at the surface and water table respectively and assuming a constant vertical heat flux of 0.033 Watts, the thermal conductivities of those 17 layers are identified.

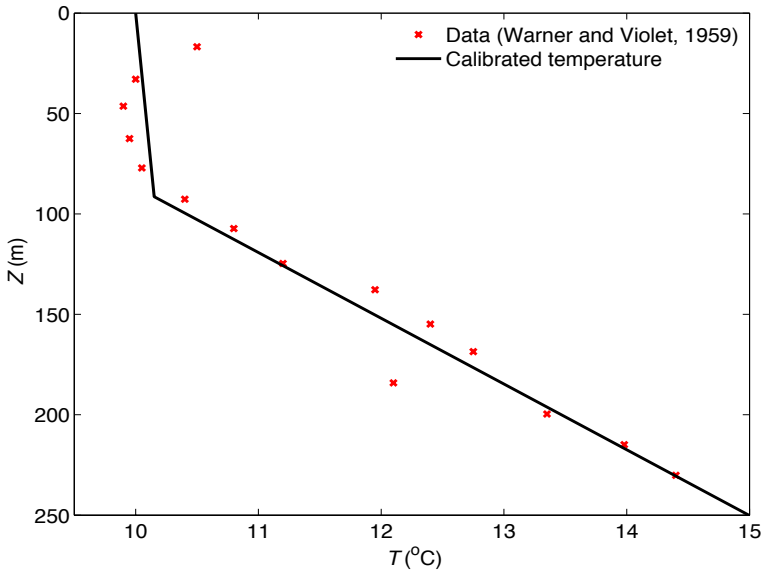

Figure 5. Veritcal temperature profile. The temperature was measured in well UCRL-3 on August 13, 1957 (Warner and Violet, 1959).

4. Modeling Results and Analyses

4.1. Model Results of Non-Proliferation Experiment

In the NPE model, the barometric pumping is the only driving force for gas-phase convection in fractures. Among many other parameters, component diffusivity, fracture aperture size, and permeability and thickness of alluvium (if there is any) dominate the detection indices (arrival time, detection window width and height). The model of Carrigan et al. (1996) is modified using USNT module (Nitao, 1998) with and without alluvium coverage. Two sets of 100 UNST models are developed for (1) possible combinations of the diffusivity and aperture size without the alluvium coverage, and (2) possible combinations of the diffusivity and alluvium permeability with the coverage. Model samples are produced using the LPTAU method in the PSUADE code (Tong, 2005).

4.1.1. Effect of Effective Diffusivity and Fracture Aperture Size. The effective (intraparticle) diffusivity is defined as the product of free diffusivity and tortuosity. In the below-boiling test, the barometric pumping of surface pressure is the only driving force for gas component release through ground surface. Figure 6 shows the concentration histories for ^{133}Xe and SF_6 at the mouth of the fracture. Pure diffusion without considering the barometric pumping never delivers ^{133}Xe to ground surface at the detection level.

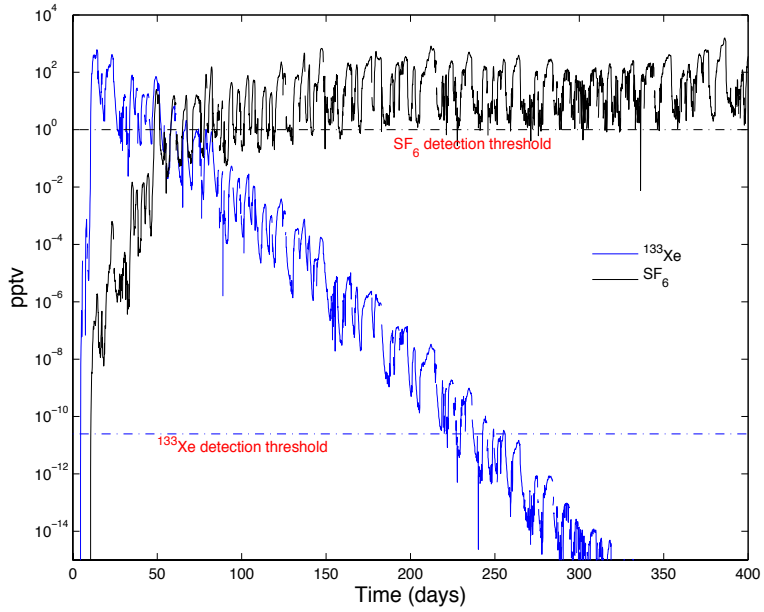

Figure 6. Concentration histories for ^{133}Xe and SF_6 at the outlet of the fracture (Figure 1b). Diffusivities for ^{133}Xe and SF_6 are respectively, $3.16{\cdot}10^{-7}$ and $7.60{\cdot}10^{-6}$. The half aperture size is $7.50{\cdot}10^{-4}$.

Taking 1 mBq m^{-3} (equivalent to $2.48{\times}10^{-11}$ ppvt in air) as the measurement threshold for ^{133}Xe, the response surface of the arrival time is constructed using the PSUADE code (Tong, 2005). The first arrival time of the threshold concentration is proportional to the diffusivity in rock matrix and inversely proportional to the fracture aperture size when the permeability in alluvium takes the logarithmic mean value. As shown in Figure 7, the effective diffusivity appears more sensitive than aperture size to the arrival time.

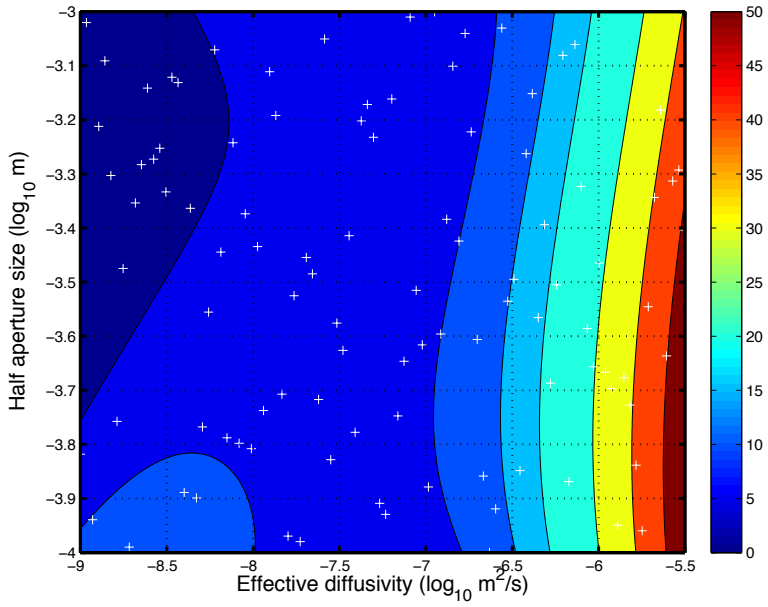

Figure 7. Arrival time (days) of ^{133}Xe as a function of effective diffusivity and half-aperture size of fracture. Note that the white "+" indicates sample locations in the space of matrix diffusivity and half-aperture size.

The detection window width is also examined as a function of the diffusivity and half-aperture size (Figures 8). These two figures 7 and 8 can be used for detecting other gas components with specific diffusivity ranges.

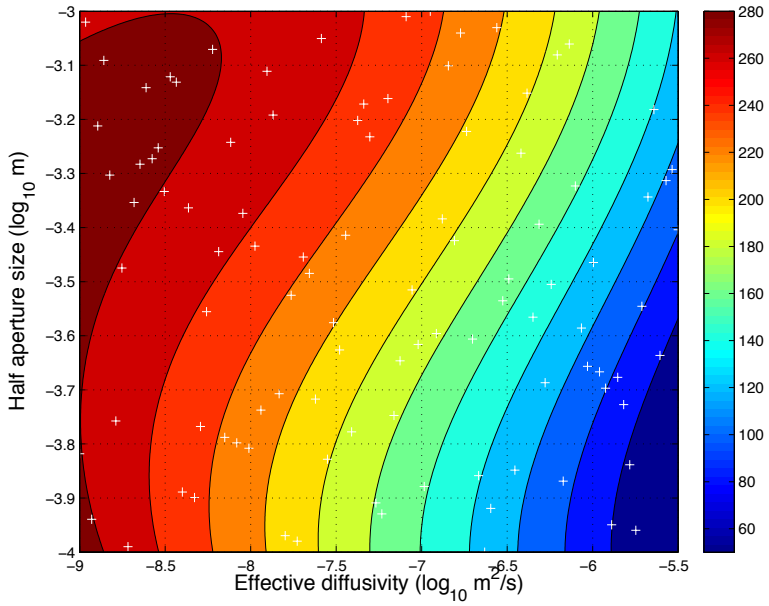

Figure 8. Detection window width (days) of ^{133}Xe as a function of effective diffusivity and half-aperture size.

4.1.2. Effect of Diffusivity and Alluvium Permeability. When the fracture aperture size is fixed with the logarithmic mean value, the detectability is evaluated in terms of matrix diffusivity and alluvium permeability. Alluvial layers or low-permeability rock on the top of the study domain reduce the effect of barometric pumping on gas-phase advection, dampen the magnitude of concentration signal, and cause a delay (phase shift) of the cyclic concentration history. Using the PSUADE code (Tong, 2005), a sensitivity analysis of detection characteristics is conducted in terms of the diffusivity and permeability.

Figures 9 and 10, show the arrival time and detection window width respectively, as functions of ^{133}Xe diffusivity and the permeability in alluvium. The white area in those figures indicates the non-detectable zone. The concentration history of ^{133}Xe on ground surface may never reach the detection threshold for high diffusivity in rock matrix and low permeability in alluvium. Although the alluvium thickness is fixed (2.0 m) in the model, it is expected that the non-detectable area grows monotonically with the thickness.

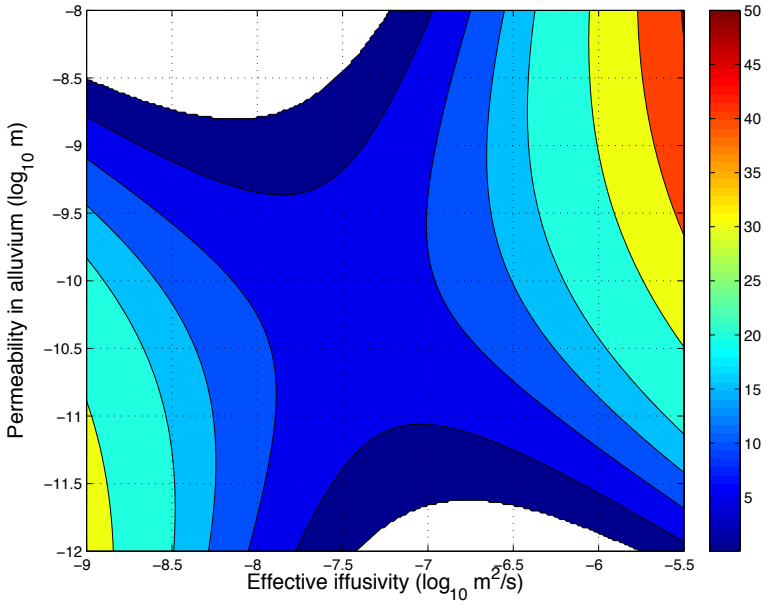

279 **Figure 9.** Arrival time (days) as a function of effective diffusivity and permeability in alluvium.

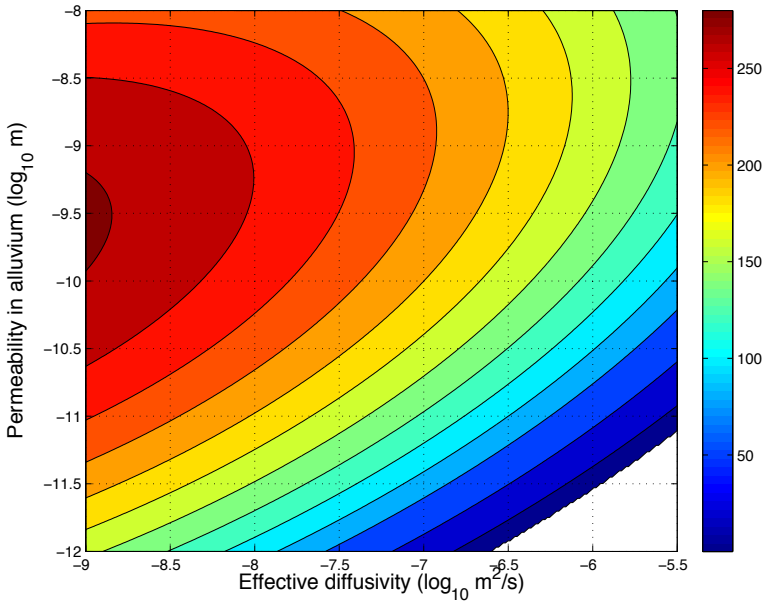

280 **Figure 10.** Detection window width (days) as a function of effective diffusivity and permeability in alluvium..

281 ## 4.2. Model Results of Rainier Test

282 In Rainier Test model, we consider two-phase, four-component transport in a dual-
283 permeability medium under thermal conditions. The main transport mechanisms include
284 gas- and liquid-phase advection, dispersion and diffusion, and vapor-liquid partitioning.
285 Test residual heat maintains the working point and surrounding area above boiling point
286 for about two years. The countercurrent flow of steam and liquid water is formed between
287 the boiling and condensation zones when the vapor and liquid fluxes are of sufficient mag-

nitude. Because of the high efficiency of latent heat transport, the temperature gradient in the heat-pipe zone is minimal, resulting in nearly isothermal conditions (Sun et al., 2010). Capillary pressures play an important role in determining gas-phase flux from the hot end to the cool end of the heat pipe, and liquid-phase flux back to the hot side.

4.2.1. Steam Expansion and Heat-Pipe Phenomenon. Prior to the chimney collapse, the total water mass is estimated using the initial saturation, porosity, and melted volume of rock within the cavity (equivalent to the puddle glass volume). The steam bubble is formed by the test heat and well contained in the cavity by the compressed and impermeable cavity wall. Immediately after cavity collapse, the steam bubble expands, under thermally induced pressure gradient, to the chimney and crushed zones (within two cavity radii). Temperature profile drops rapidly with the radial distance from the cavity. Therefore, most water outside the cavity after detonation will initially be in the liquid phase. The puddle zone temperature, however, will be much higher than the boiling point.

As shown in Figure 11, a geologic heat pipe is formed by the countercurrent flow of steam in fractures and liquid water in matrix between the boiling and condensation zones. The 8-meter-wide plateau on temperature profile results from the gas-phase flux from the hot end to the cool end of the heat pipe and the liquid-phase flux toward to the working point. The steam bubble grows from the working point and shrinks after reaching the maximum size. As liquid water supplies to the chimney zone, the steam production results in high pressure and drives xenon and argon away from the chimney.

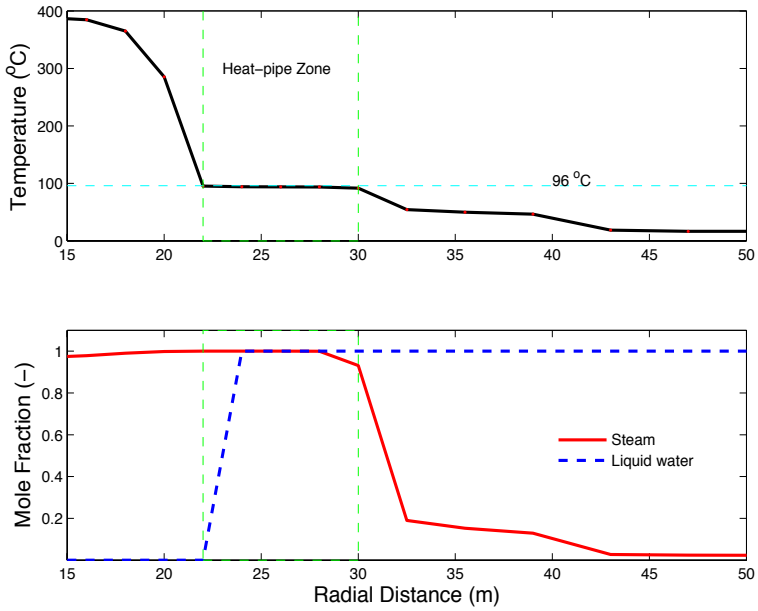

Figure 11. Temperature profile for $z = 274.3$ m and $t = 60$ d. The dashed green box represents the heat-pipe zone, in which gas phase flows from left to right in fractures and liquid phase flows from right to left in matrix by capillary pressure. The temperature in the heat-pipe zone remains constant.

Figure 12 shows the heat-pipe zone defined between the the boiling front (red line) and condensation front. The heat-pipe zone develops at 1 day (Figure 12a) and reaches 8 meter wide (at z=274.3 m) at 60 days. The inner line bounds the steam zone while the outer line holds the liquid water.

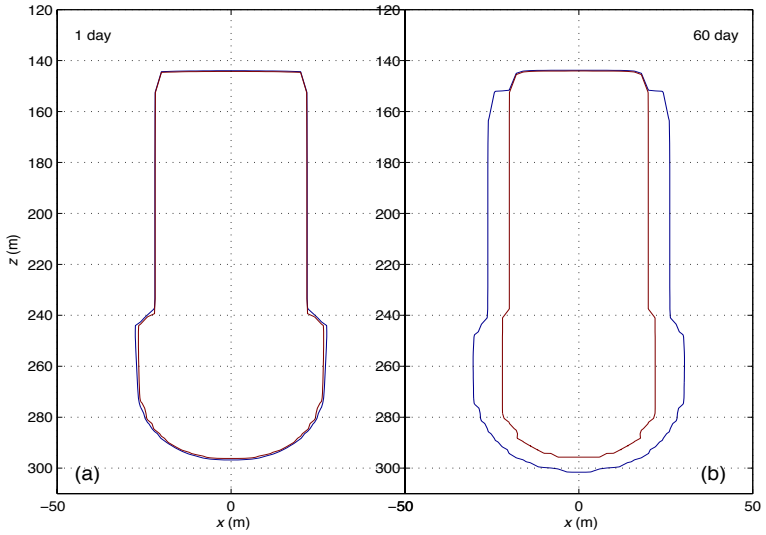

Figure 12. Heat pipe zone at 1 day (a) and 60 days (b). The heat pipe zone is defined between the boiling front (red line) and condensation front (blue line).

4.2.2. Sample Concentrations. Radioactivities of ^{133}Xe and ^{37}Ar and mole fractions of water and air are measured at depth of 11.5, 17.5, 46, and 102 m on the vertical central line (x=0, Figure 1). As shown in Figures13 and 14, both ^{133}Xe and ^{37}Ar reach their peak concentrations within a few hours and then decay accordingly to their half-lives. The detection window width for ^{133}Xe is about 260 days. The concentration history of ^{133}Xe at those points (at depth of 11.5, 17.5, 46, and 102 m) is dominated by the barometric boundary condition at low concentration magnitudes. Figure 13 shows the different mechanisms before and after 260 days. The thermally driven advection and the first-order reaction control ^{133}Xe concentration histories in the first 260 days. When the concentration drops to a certain magnitude near threshold level, the effect of barometric-pumping boundary with concentration of 1.0×10^{-30} (mole fraction) becomes more apparent. For this reason, ^{133}Xe concentration after 260 days fluctuates with the boundary pressure. However, because of the longer half-life of ^{37}Ar, its concentration magnitude is much higher than the boundary concentration and the surface-boundary effect does not dominate the concentration history of ^{37}Ar with the simulation time (500 days).

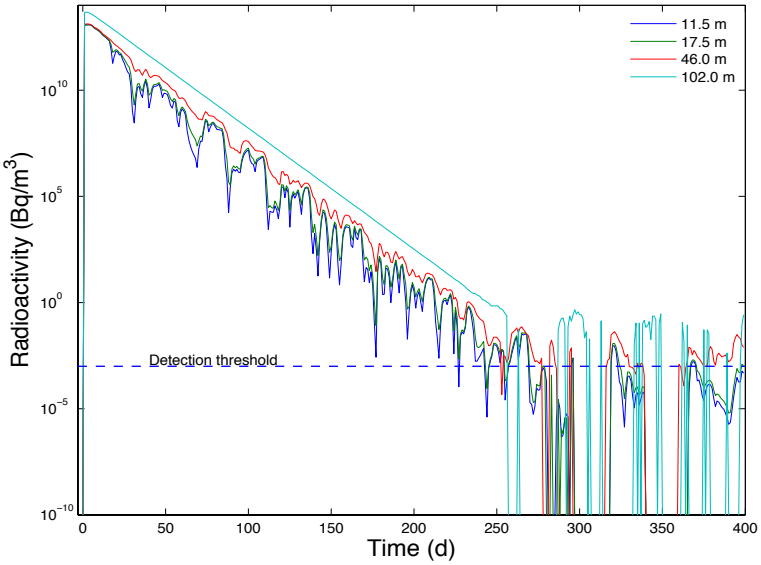

Figure 13. Concentration histories of xenon-133 at depth of 11.5, 17.5, 46, and 102 m.

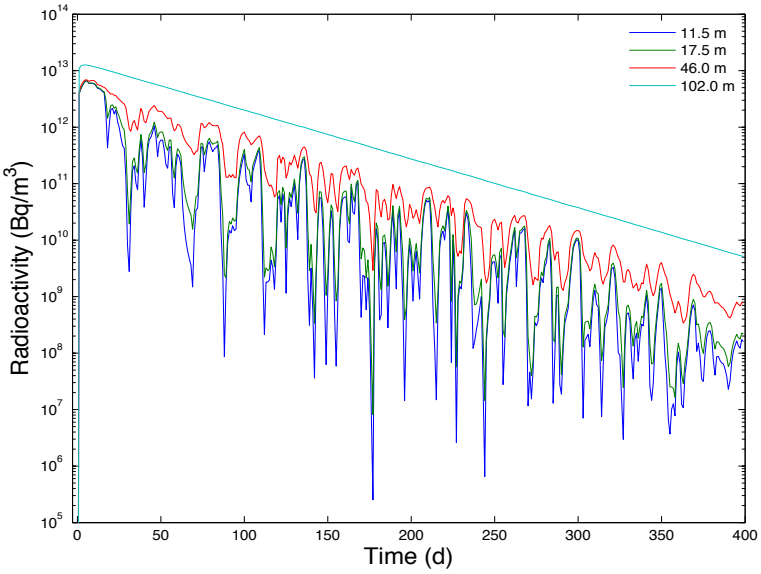

Figure 14. Concentration histories of argon-37 at depth of 11.5, 17.5, 46, and 102 m.

Figures 15 and 16 show the concentration histories of water and air at four locations. These concentration profiles are mainly controlled by barometric pressure boundary and steam production by test residual heat. The water mole fraction keeps the highest in the chimney and lowest away from the working point.

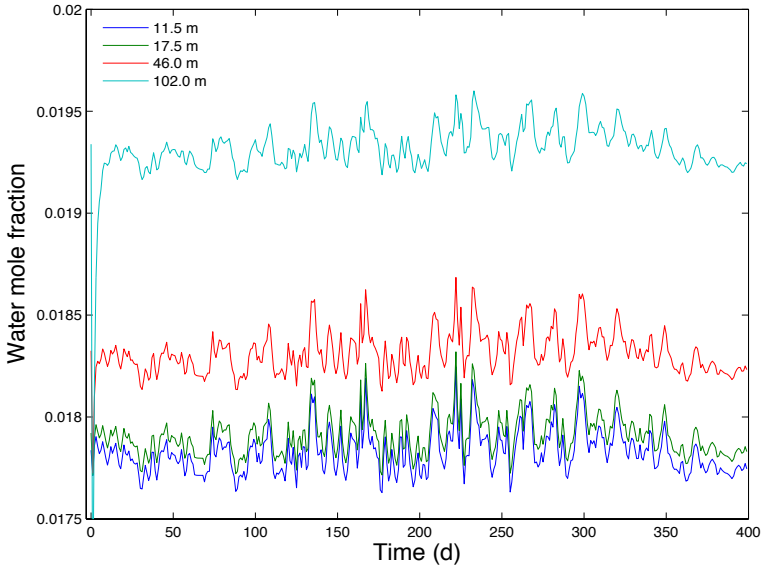

335 **Figure 15.** Concentration histories of water at depth of 11.5, 17.5, 46, and 102 m.

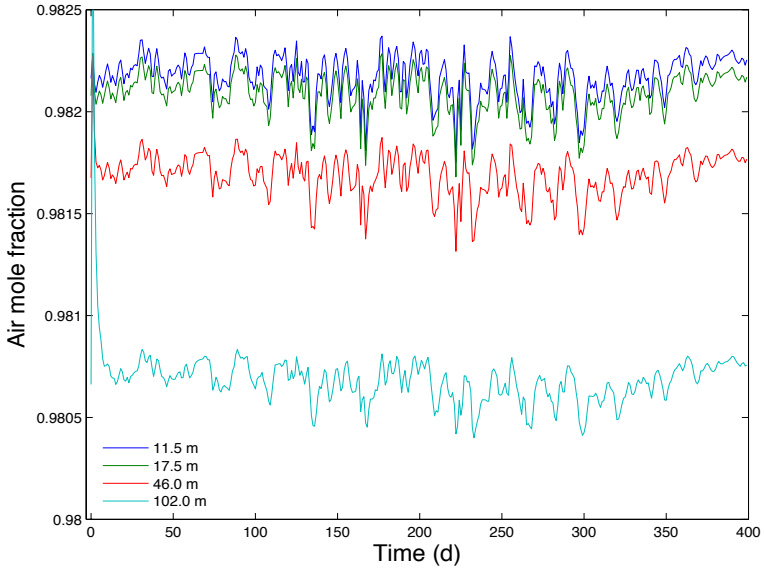

336 **Figure 16.** Concentration histories of air above chimney at depth of 11.5, 17.5, 46, and 102 m.

337 **4.2.3. Spatial Distributions of Noble Gas Components.** Test-related ^{133}Xe and
338 ^{37}Ar concentrations (Bq/m^3) at various times reflect the transport processes in the fractured
339 rock. Figures 17 and 18 show the ^{133}Xe and ^{37}Ar plumes at 1 day and 100 days. The ^{37}Ar
340 plume is widely spread because of its higher diffusivity.

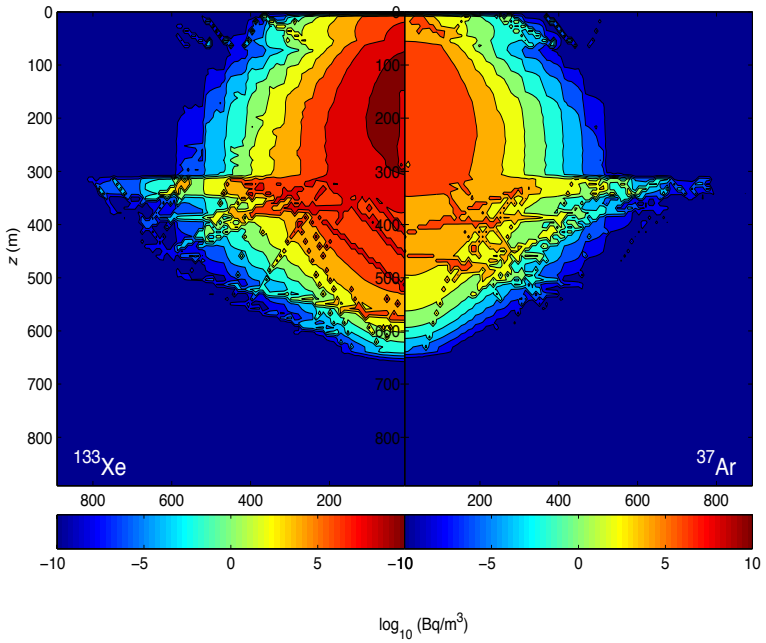

Figure 17. Contour plots of ^{133}Xe and ^{37}Ar activities (Bq/m^3) at 1 day. Note that the half-symmetry domain of ^{133}Xe plume is flipped to the left for the comparison purpose.

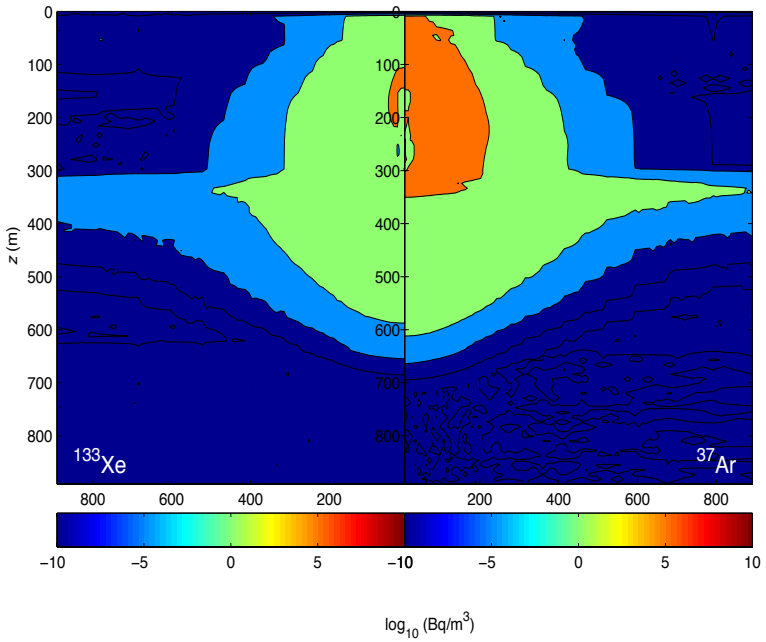

Figure 18. Contour plots of ^{133}Xe and ^{37}Ar activities (Bq/m^3) at 100 days.

Figures 19 and 20 show the distribution of the mole fraction of steam and air at 1 day and 100 days. The steam bubble is expanded from the working point in the chimney and mainly contained within the boiling front. Both boiling and condensation fronts expand and drive the test-related noble gas away from the chimney.

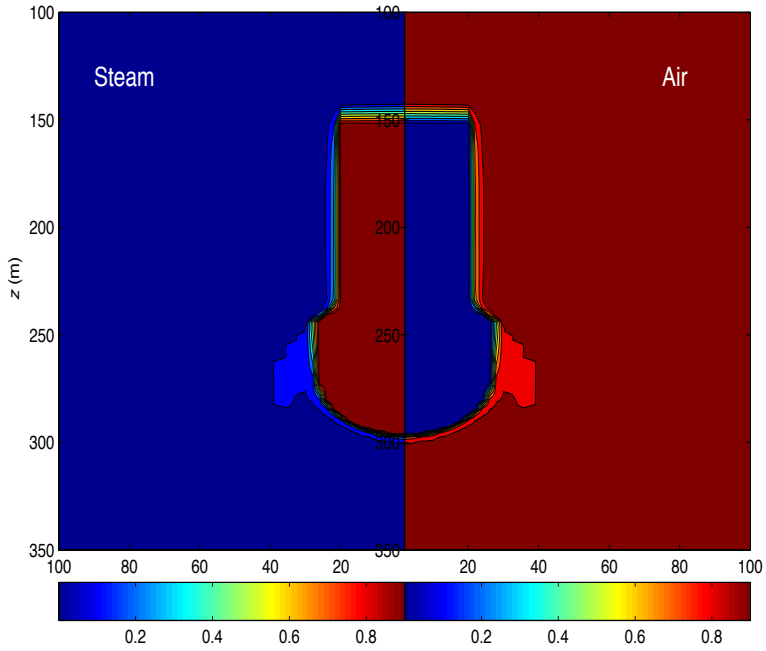

Figure 19. Contour plots of steam and air at 1 day.

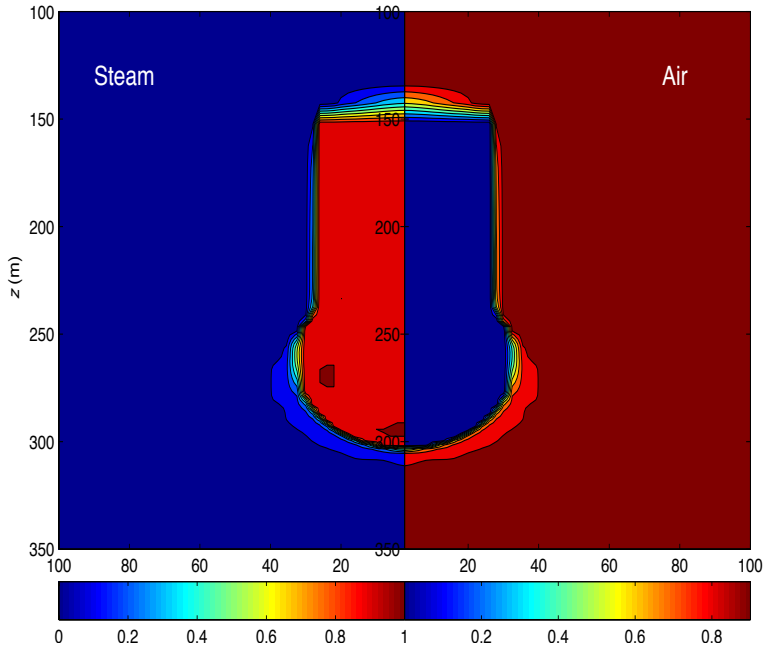

Figure 20. Contour plots of steam and air at 100 days.

5. Conclusions

The detectability of noble gas ^{133}Xe and ^{37}Ar is quantitatively characterized using (1) arrival time, (2) detection window width, and (3) detection window height. The transport of ^{133}Xe and ^{37}Ar is described by a single-gas-phase model and a two-phase multi-component

model. In this study, we demonstrated the processes of ^{133}Xe and ^{37}Ar transport in fractured rock.

When the temperature is below the boiling point and the subsurface system is sufficiently dry, the system can be modeled as a single-gas-phase transport. Then, the barometric pumping becomes the major driving force to deliver ^{133}Xe and ^{37}Ar to ground surface. If the fractured rock is not covered by alluvia, the diffusivity in rock matrix and fracture aperture size are sensitive parameters contributing the detectability of noble gases at ground surface. When the ground surface is covered by alluvia, the permeability in the overburden layer replaces the fracture aperture size to become a sensitive parameter. The detection zone is provided in possible ranges of sensitive parameters.

The above-boiling test is modeled as a two-phase and multi-component transport. Steam production and bubble expansion are the major process to drive noble gas components to ground surface. Geologic heat pipe keeps constant (at boiling point) from its boiling front to the condensation front. Capillary-pressure in the rock matrix drives liquid water to move toward the boiling front and the pressure gradient elevated by phase change (steam production) drives steam away from the chimney through fractures. The steam bubble becomes a major driver for noble gas transport. The arrival time is usually shorter compared to that in the single-gas model. After the temperature in the chimney drops below boiling point, the barometric pumping takes over the role as the major driving force.

Both models show that the detection window width for ^{133}Xe is smaller that for ^{37}Ar because of the shorter half life. To take advantage of ^{133}Xe detection sensitivity, the monitoring is suggested at the early stage. This study is limited to two specific tests. Further study is necessary for a wide range of yields and geological conditions.

Acknowledgements

The authors wish to thank xxx at Lawrence Livermore National Laboratory for his careful review and helpful comments that led to an improved manuscript. This research was partially funded by the program of ?, U.S. Department of Energy and performed under the auspices of the U.S. Department of Energy by Lawrence Livermore National Laboratory under Contract No. DE-AC52-07NA27344.

References

Auer, L.H., N.D. Rosenberg, K.H. Birdsell, E.M. Whitney, The effect of barometric pumping on contaminant transport, *J. Contam. Hydrol.*, 24, 145–166, 1996.

Auer, M., A. Axelsson, X. Blanchard, B.W. Bowyer, G. Brachet, Y. Bulowski, K. Elmgren, J.P. Fontaine, W. Harms, J.C. Hayes, T.R. Heimbigner, J.I. McIntyer, M.E. Panisko, Y. Popov, A. Ringbom, H. Sartorius, S. Schmid, J. Schulze, C. Schlosser, T. Taffary, W. Weiss, B. Wernsperger, Intercomparison experiments of systems for the measurement of xenon radionuclides in the atmosphere, *Appl. Rad. Isotopes*, 60, 863–877, 2004.

Auer, M., T. Kumberg, H. Sartorius, B. Wernsperger, C. Schlosser, Ten years of development of equipment for measurement of atmospheric radioactive xenon for the verification of the CTBT, *Pure Appl. Geophys.*, DOI 10.1007/s00024-009-0027-y, 2010.

Bowyer, T.W., C. Schlosser, K.H. Abel, M. Auer, J.C. Hayers, T.R. Heimbigner, J.I. McIntyre, M.C., Panisko, P.L. Reeder, H. Satorius, J. Schulze, W. Weiss, Detection and analysis of xenon isotopes for the comprehensive nuclear-test-ban treaty international monitoring system, *J. Environ. Radioactivity*, 59, 139–151, 2002.

Buscheck, T.A., N.D. Rosenberg, J. Gansemer, Y. Sun, Thermohydrologic behavior at an underground nuclear waste repository, *Water Resour. Res.*, 38(3), 1431–1447, 2002.

Carle, S.F., M. Zavarin, Y. Sun, G.A. Pawloski, Evaluation of hydrologic source term processes for underground nuclear tests in Yucca Flat, Nevada Test Site: Carbonate Tests, LLNL-TR-403485, 2008.

Carrigan, C.R., R.A. Heinle, G.B. Hudson, J.J. Nitao, J.J. Zucca, Trace gas emissions on geological faults as indicators of underground nuclear testing, *Nature*, 382(6591), 1996.

Carrigan, C.R., Calibration and testing of predictive models of gas-phase transport in the vadose zone: an example from the Nevada Test Site, Lawrence Livermore National Laboratory, UCRL-133586, 1999.

Carrigan, C.R., The non-proliferation experiment and gas sampling as an on-site inspection activity: a progress report, Lawrence Livermore National Laboratory, UCRL-JC-117752, 1994.

Clever, H. L., Ed., *Helium and Neon, IUPAC Solubility Data Series*, Vol. 1, Pergamon Press, Oxford, 1979.

Clever, H. L., Ed., Argon, IUPAC Solubility Data Series, Vol. 4, Pergamon Press, Oxford, 1980.

de Marsily, G., *Quantitative Hydrogeology: Groundwater Hydrology For Engineers*, Academic Press, 1986.

Dresel, P.E., S.R. Waichler, Evaluation of xenon gas detection as a means for identifying buried transuranic waste at the radioactive waste management complex, Idaho National Environmental and Enginerring Laboratory, Pacific Northwest National Laboratory, PNNL-14617, 2004

Ekwrzel, B., *LLNL Isotope Laboratories Data Manual*, Lawrence Livermore National Laboratory, UCRL-TR-203316, 2004.

Ho, C.K., Models of fracture-matrix interaction during multiphase heat and mass flow in unsaturated fractured porous media, Sixth Symposium on Multiphase Transport in Porous Media, Dallas, TX, Nov. 16–21, 1997.

Holocher, J., F. Peeters, W. Aeschbach-Hertig, M. Hofer, M.S. Brennwald, W. Kinzelbach, R. Kipfer, Experimental investigation on the formation of excess air in quasi-saturated porous media, *Geochim. Cosmochim. Ac.*, 66(23), 4103–4117, 2002.

Lee, E.L., H.C. Hornig, J.W. Kury, Adiabatic expansion of high explosive detonation products, Lawrence Livermore National Laboratory, TID-4500 UC-4, 1968.

Lindstrom, F.T., D.E. Cawlfield, L.E. Baker, Sensitivity analysis of the noble gas transport and fate model: CASCADR9, DOE/NV/11432-129, 1994.

Martinez, M.J., R.H. Nilson, Estimates of barometric pumping of moisture through unsaturated fractured rock, *Transport Porous Med.*, 36, 85–119, 1999.

Mullen, A.A., J. Barth, Noble gas and tritium-in-air offsite environmental monitoring program summary from 1970-1995, US EPA, EPA-402-R-99-005, 1999.

Neeper, D.A., A model of oscillatory transport in granular soils, with application to barometric pumping and earth tides, *J. Contam. Hydrol.*, 48, 237–252, 2001.

Neeper, D.A., Investigation of the vadose zone using barometric pressure cycles, *J. Contam. Hydrol.*, 54, 59–80, 2002.

Nilson, R.H., E.W. Peterson, K.H. Lie, Burkhard, N.R., J.R. Hearst, Atmospheric pumping: a mechanism causing vertical transport of contaminant gases through fractures permeabile media, *J.Geophys. Res.*, 96(B13), 21933-21948, 1991.

Nitao, J.J., User's manual for the USNT module of the NUFT code, version 2 (NP-phase, NC-component, thermal), Lawrence Livermore National Laboratory, UCRL-MA-130653, 1998.

Pruess, K., Numerical codes for continuum modeling of gas transport in porous media, Ho, C. and Webb, S. (eds.), *Gas transport in porous media*, 213–220, Springer, 2006.

448 Rossabi, J., Analyzing barometric pumping to characterize subsurface permeability, Ho, C.
449 and Webb, S. (eds.), *Gas transport in porous media*, 279–290, Springer, 2006.
450 Saey, P.R.J., The influence of radiopharmaceutical isotope production on the global ra-
451 dioxenon background, *J. Environ. Radioactivity*, 100, 396–406, 2009.
452 Smith, C.F., R.W. Tylor, Rio Blanco gas quality analysis and evaluation program status
453 report, Lawrence Livermore National Laboratory, UCRL-74868, 1973.
454 Sun, Y., T.A. Buscheck, K.H. Lee, Y. Hao, S.C. James, Modeling thermal-hydrological
455 processes for a heated fractured rock system: impact of a capillary-pressure maximum,
456 *Transport Porous Med.*, 83, 501–523, 2010.
457 Tidwell, V., Scaling issues in porous and fractured media, Ho, C. and Webb, S. (eds.), *Gas*
458 *transport in porous media*, 201–212, Springer, 2006.
459 Tompson, A.F.B., On the evaluation of hydrologic source term behavior for underground nu-
460 clear tests conducted at rainier Mesa and Shoshone Mountain, Nevada Test Site, Lawrence
461 Livermore National Laboratory, Livermore, California, 2010.
462 Tong, C., *PSUADE User's Manual*, Lawrence Livermore National Laboratory, LLNL-SM-
463 407882, 2005.
464 Warner, S.E., C.E. Violet, Properties of the environment of underground nuclear detona-
465 tions at the Nevada Test Site, UCRL-5542, Lawrence Radiation Laboratory, Livermore,
466 California, 1959.
467 Webb, S.W., Gas-phase diffusion in porous media, SAND96-1197, UC-403, 1996.
468 Wu, Y., K. Pruess, P. Persoff, Gas flow in porous media with Klinkenberg effects, *Transport*
469 *Porous Med.*, 32, 117–137, 1998.
470 Wyatt, D.E., D.M. Richers, R.J. Pirkle, Barometric pumping effects on soil gas studies for
471 geological and environmental characterization, *Environ. Geol.*, 25(4), 243-250, 1995.

This preprint was prepared with Yunwei Sun's LaTeX macros v4. File ctbt˙v3 formatted August 24, 2011.